P5.19 A COMPARISON OF TROPICAL CYCLONE HYDROMETEOR PROFILES FROM TRMM, AIRBORNE RADAR, AND HIGH-RESOLUTION SIMULATIONS

Robert Rogers[1], Michael Black[1], Frank Marks[1], Krystal Valde[2], and Shuyi S. Chen[3]

[1]NOAA/AOML Hurricane Research Division, Miami, FL 33149
[2]CIMAS, University of Miami
[3]Division of Meteorology and Physical Oceanography, RSMAS, University of Miami

1. INTRODUCTION

Tropical cyclone intensity and rainfall are ultimately dependent on the magnitude and distribution of the release of latent heat within the storm's circulation, highlighting the importance of obtaining accurate estimates and predictions of latent heat release. The TRMM satellite has been a valuable tool in providing measurements of the vertical profiles of reflectivity and hydrometeor mixing ratio. These profiles are key to determining latent heating profiles, since many algorithms for determining latent heating profiles rely on the output from cloud-scale numerical models to link the measured hydrometeor profiles with vertical velocity and derive the latent heating profiles (e.g., Tao et al. 2001). The uncertainty in the latent heating profiles is thus to a large extent dependent on the uncertainties in the linkages between vertical velocity and hydrometeor mixing ratios present in the numerical models. Comparisons between these types of models and independent observations can provide a means of quantifying this uncertainty and lead to improved latent heating profiles

2. METHODOLOGY

Statistics of reflectivity and vertical motion are compared for three different datasets: PR reflectivity data from 34 passes over 18 tropical cyclones, vertical incidence tail Doppler radar data from 233 radial legs within 9 different tropical cyclones, and output from 1.67-km grid length MM5 simulations of Hurricanes Bonnie (1998) and Floyd (1999). Each dataset was sorted into eyewall, rainband, and stratiform regions based on reflectivity (TRMM data) and reflectivity and vertical velocity (VI and model data) (Fig. 1). Reflectivity means, distributions, and vertical velocity-binned averages of reflectivity are calculated and presented here.

The microphysical parameterization scheme used in the simulations is a modified version of the Tao-Simpson (Tao and Simpson 1993) cloud microphysics scheme for all four meshes. The Tao-Simpson scheme, which was modified from Lin et al. (1983), is a bulk three-class single-moment ice scheme that contains prognostic equations for cloud water (ice), rainwater (snow), and hail/graupel, and it allows for the existence of supercooled water. This scheme includes the processes of condensation/ evaporation, freezing/melting, sublimation/deposition, autoconversion (i.e., aggregation) of cloud water (ice, snow) to form rainwater (snow, hail/graupel), collection by rainwater (snow), and accretion.

* *Corresponding author address:* Robert Rogers, NOAA/AOML Hurricane Research Division, e-mail: Robert.Rogers@noaa.gov

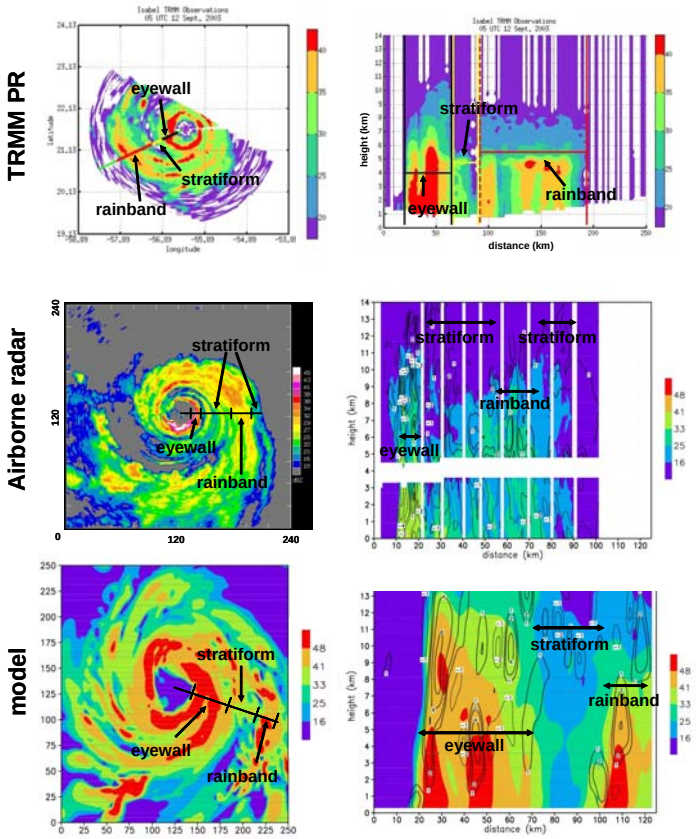

Figure 1. Examples of sorting scheme for each dataset. Reflectivity plan-view (left column, reflectivity (dBZ), shading) and vertical cross sections (right column, reflectivity (dBZ, shaded), vertical velocity (m s^{-1}, contour, for airborne radar and model)) are shown. Examples shown are Hurricane Isabel (2003) for TRMM PR, Hurricane Olivia (1994) for airborne radar, and Hurricane Floyd (1999) for MM5 simulation. Areas identified as eyewall, rainband, and stratiform are identified.

3. RESULTS

Figure 2 shows profiles of mean reflectivity for the eyewall and stratiform regions for each of the three datasets. The mean reflectivity in the eyewall is higher than

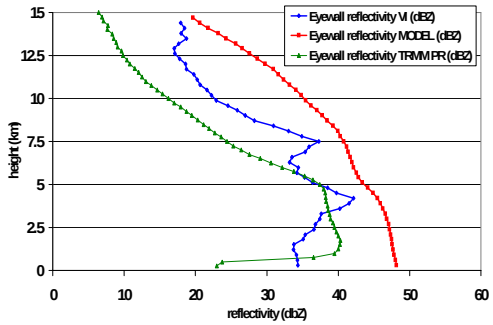

(a)

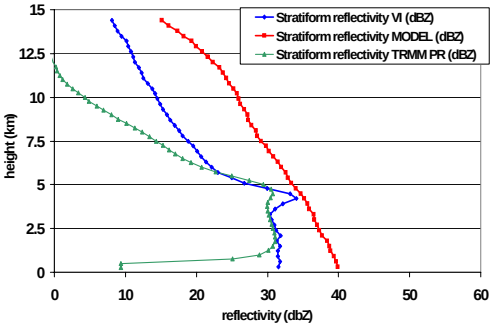

(b)

Figure 2. Vertical profiles of mean reflectivity (dBZ) for TRMM PR (green), airborne radar (blue), and model-generated reflectivity (red). (a) eyewall region; (b) stratiform region

the mean reflectivity in the stratiform region for each of the three datasets. The TRMM PR mean reflectivity is comparable to the airborne reflectivity below the melting level (here about 4.5 km). Above the melting level, the reflectivity from the TRMM PR decreases faster with height than the airborne radar. This is especially the case for the stratiform region. In both the eyewall and the stratiform region, the reflectivity from the simulations is higher than the observed reflectivity, for both the TRMM PR and the airborne radar datasets. This high bias, commonly-seen in mesoscale model simulations of tropical cyclones (e.g., Liu et al. 1997; Rogers et al. 2003), persists throughout the depth of the troposphere. Another difference between the model and the observations is that the mean reflectivity decreases less rapidly with height than either the TRMM PR or the airborne radar.

Figure 3 shows a comparison of model output and observations using contoured frequency by altitude diagrams (CFADs; Yuter and Houze 1994). These diagrams essentially plot the variation of probability distribution functions with height. Figure 3 shows CFADs of reflectivity for the TRMM PR, airborne radar, and simulations. The maximum frequency of reflectivity (i.e., the mode) for the TRMM observations are intermediate in value between the airborne radar and simulations. For example, modal values of reflectivity in the lowest 1-2 km are 40 (30) dBZ for the eyewall(stratiform) regions in TRMM, 30 (25) dBZ for the eyewall (stratiform) regions in the airborne radar, and 45 (38) dBZ for the eyewall (stratiform) regions in the simulations. Similar relationships hold for higher

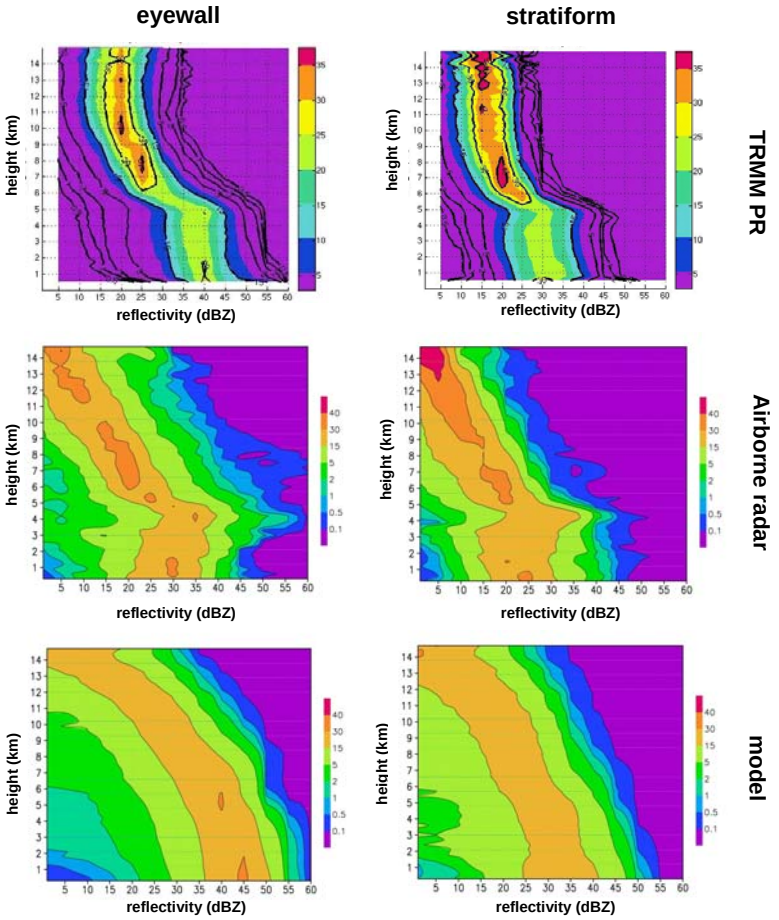

Figure 3. Contoured frequency by altitude diagrams (CFADs) of reflectivity (shaded, %) for TRMM PR, Airborne radar, and model data sorted by region. Values of 0.5, 1, and 2 are contoured on TRMM CFAD.

altitudes as well. In general, the modal and peak (i.e., top 0.1% of distribution) values of reflectivity are highest in the simulations, again reflecting the high bias commonly seen in tropical cyclone simulations. The slower decrease with height of reflectivity in the simulations compared with both the TRMM PR and airborne radar is again evident in the CFADs.

A similar comparison of CFADs for vertical motion is presented in Figure 4 for the airborne radar and simulations. As in Black et al. (1996), the majority of observed eyewall vertical motions (Fig. 1a) are weak ($|w| < 2$ m s^{-1}), but a small fraction (1-2%) of up- and downdrafts exceed 6 m s^{-1}. The distributions are fairly constant with height below the melting level, but they broaden with height above, indicating strong up- and downdrafts aloft for the extreme events (from –12 m s^{-1} to 12 m s^{-1}). Modal values of vertical motion are slightly negative in the lowest 2 km, but above 9 km they are clearly positive, reflecting the loss of hydrometeors and reduction in water loading in the upper levels. The distribution of observed vertical motion is narrower for the stratiform region, indicating a smaller proportion of extreme values and a larger proportion of weak values. In contrast to the observations, the simulated vertical motion CFADs show a narrower distribution of vertical velocities. The majority of simulated up- and downdrafts are weak, similar to the

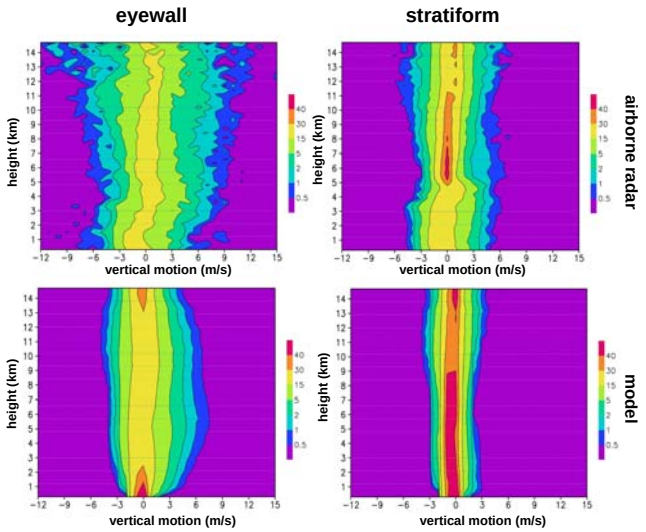

Figure 4. CFADs of vertical velocity (%) for airborne radar and model data sorted by region.

observations, but values of the maxima are less than the observed values. In the upper troposphere, the vertical motion distribution narrows with height, in contrast to the observations.

Figure 5 shows the vertical distribution of airborne radar and model mean reflectivity binned by vertical velocity. There is a suggestion of a weak relationship between reflectivity and vertical motion in the radar observations. Between 3 and 5 km altitude, observed reflectivity values increase slowly as upward motion increases from 0 to 9 m s^{-1} (e.g., increasing from 37 dBZ for the 0 m s^{-1} bin to 47 dBZ for the 6 m s^{-1} bin at the 4-km level). Above the melting level, between 7 and 12 km altitude, there is again a weak relationship between vertical motion and reflectivity, for both up- and downdrafts. The relationship between vertical motion and reflectivity is much stronger for the simulations, however. The slope of the relationship is very pronounced for the weak vertical motions (i.e., between –2 and 2 m s^{-1}), and there is a noticeable slope even for vertical motion values exceeding 9 m s^{-1}.

4. FUTURE WORK

The differences between the observations and the simulations shown here indicate possible differences in the relationship between hydrometeor mixing ratio and vertical motion. Such a difference is important for latent heating algorithms, since many such algorithms use latent heating profiles derived from cloud-resolving models that use microphysical parameterizations similar to that used in the simulations here. If there is a bias in the parameterization scheme that is reflected in the relationship between mixing ratio and vertical motion, then that may be reflected in the latent heating algorithm as well.

Future work will involve testing the accuracy of the latent heating profiles used with the TRMM data. This can be done by first calculating hydrometeor vertical profiles from the airborne radar using reflectivity-mass relationships and comparing these profiles with TRMM TMI-generated hydrometeor profiles. Correlations between vertical motion and hydrometeor mass from the airborne radar can then be calculated, and these correlations can be applied to the TRMM data. They can then be compared with the correlations from the simulations and the latent heating profiles generated from the TRMM algorithms. Any differences that exist between the datasets can be identified and possible corrections implemented.

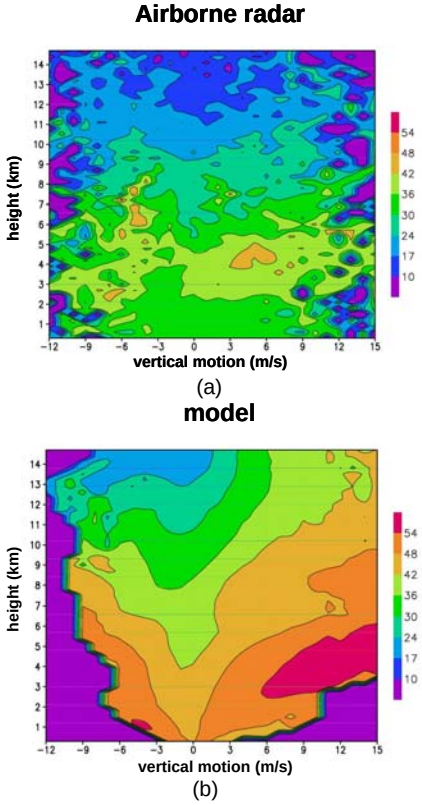

Figure 5. Mean eyewall reflectivity (shading, dbZ) stratified by (a) Doppler-derived and (b) model-derived vertical motion bins for all storms.

5. ACKNOWLEDGEMENTS

This work was supported by a NASA TRMM research grant to HRD and to University of Miami, grant number NAG5-10963.

6. REFERENCES

Lin, Y.-L., R.D. Farley, and H.D. Orville, 1983: Bulk parameterization of the snow field in a cloud model. J. Climate Appl. Meteor., 22, 1065-1092.

Liu, Y., D.-L. Zhang, and M.K. Yau, 1997: A multiscale numerical study of Hurricane Andrew (1992). Part I: Explicit simulation and verification. Mon. Wea. Rev., 125, 3073-3093.

Rogers, R.F., S.S. Chen, J.E. Tenerelli, and H.E. Willoughby, 2003: A numerical study of the impact of vertical shear on the distribution of rainfall in Hurricane Bonnie (1998). Monthly Weather Review, 131, 1577-1599.

Tao, W.-K., and J. Simpson, 1993: The Goddard cumulus ensemble model. Part I: Model description. Terr. Atmos. Oceanic Sci., 4, 35-72.

Tao, W.-K., S. Lang, W. S. Olson, R. Meneghini, S. Yang, J. Simpson, C. Kummerow, E. Smith and J. Halverson, 2001: Retrieved vertical profiles of latent heat release using TRMM rainfall products for February 1998. J. App. Meteor., 40, 957–982.

Yuter, S.E., and R.A. Houze, Jr., 1994: Three-dimensional kinematic and microphysical evolution of Florida cumulonimbus. Part III: Vertical mass transport, mass divergence, and synthesis. Mon. Wea. Rev., 123, 1964-1983.